Reactive Polymer Interfaces: How Reaction Kinetics Depend on Reactivity and Density of Chemical Groups

Ben O'Shaughnessy*

Department of Chemical Engineering, Columbia University, New York, New York 10027

Dimitrios Vavylonis

Department of Physics, Columbia University, New York, New York 10027

Received June 8, 1998; Revised Manuscript Received December 30, 1998

ABSTRACT: We present a systematic theory of polymer reaction kinetics at an interface separating two immiscible melts, A and B, in each of which a fraction of chains carry reactive end groups. We consider arbitrary values of local group reactivity, Q_b, and reactive group densities in either bulk, n_A^∞ and n_B^∞, with the convention $n_A^\infty \leq n_B^\infty$. At short times reaction kinetics are second order in bulk densities. Initially, kinetics are of simple mean field type, with surface density of reaction product after time t given by $R_t \approx Q_b h a^3 t n_A^\infty n_B^\infty$ where h is the interface width and a reactive group size. If Q_b exceeds a density-dependent threshold a transition occurs, at a time less than the longest polymer relaxation time τ, to second order diffusion-controlled (DC) kinetics with $R_t \approx x_t^4 n_A^\infty n_B^\infty$. Here x_t is the rms monomer displacement. Logarithmic corrections arise in marginal cases. This leads to $R_t \sim t/(\ln t)$ for unentangled chains, while for entangled melts consecutive regimes $R_t \sim t/(\ln t)$, $R_t \sim t^{1/2}$ and $R_t \sim t/(\ln t)$ exist. Which regimes are realized depends on Q_b and n_B^∞. At long times, a transition occurs to *first-order* DC kinetics. The reaction rate, $R_t \approx x_t n_A^\infty$, is determined by the more *dilute* A side, where a density depletion hole of size x_t develops at the interface. For high reactive chain densities on the B side ($n_B^\infty R^3 > 1$ where R is polymer coil size), and for Q_b sufficiently large, these kinetics onset before τ. Then $R_t \sim t^{1/4}$ for unentangled melts, while for entangled cases consecutive regimes $R_t \sim t^{1/4}$, $R_t \sim t^{1/8}$, and $R_t \sim t^{1/4}$ arise, some or all of which may be realized depending on Q_b and n_B^∞. The final first-order regime is always governed by center of gravity diffusion, $R_t \sim t^{1/2}$. At a certain time scale the interface saturates with AB copolymer product and reactions are strongly suppressed. This prevents the onset of the long time first-order DC regime if the reactivity is very small, $Q_b < Q_b^\dagger$ with $Q_b^\dagger \sim 1/N^{1/2}$ (unentangled melts) or $Q_b^\dagger \sim 1/N^{3/2}$ (entangled).

I. Introduction

This paper is a theoretical investigation of the kinetics of polymer−polymer reactions occurring at an interface separating two thermodynamically immiscible polymer melt phases A and B (see Figure 1). A certain fraction of the A and B chains bear chemically reactive end groups and can react with chains in the other phase in the interfacial region only. Reactions produce A−B copolymers which eventually crowd the interface. The importance of such systems derives both from fundamental issues in polymer interfacial science and from the many technologically important applications. In the reactive reinforcement of polymer interfaces,[1−4] A−B copolymer products serve as bridges, enhancing the interfacial fracture toughness and yield stress after cooling.[5−7] Commercial applications entail the simultaneous mechanical mixing of the two melts ("reactive processing"), reactions occurring at interfaces separating droplets from the continuous phase. In addition to their direct reinforcing effect, the interfacial copolymer products also promote the mixing itself, apparently both by suppression of droplet coalescence rates and through surface tension reduction.[8−11]

A number of recent theoretical and numerical studies[12−16] have addressed these interfacial reaction kinetics. These studies focused on a small fraction of the available parameter space. They emphasized the limit of "infinitely" reactive groups, i.e. local chemical reactivities Q_b of order $1/t_a$ where t_a is the monomer relaxation time. (The definition of Q_b is the reaction rate *given* two reactive groups are in contact.) In fact, such Q_b values are realized only for exotic species such as radicals (or electronically excited groups as in model photophysical systems[17,18]) while chemical reactivities

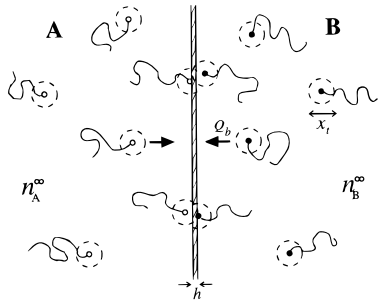

Figure 1. Interface of width h separating bulk melts A and B. Initial reactive chain densities are n_A^∞ and n_B^∞. We adopt the convention $n_A^\infty \leq n_B^\infty$. For unequal densities, the smaller A density governs long time reaction rates whereas the higher B density determines characteristic time scales. A−B reactions are confined to the interface, each reaction producing an AB diblock copolymer. For sufficiently high local reactivity Q_b, the reaction probability for a pair which was initially close enough to have diffused and met within time t reaches unity at a time scale t_2^*. For $t > t_2^*$ reactions are confined to those pairs whose exploration volumes (indicated here by dashed lines) overlap at time t at the interface. Thus R_t is the number of such pairs per unit area, $R_t \approx n_A^\infty n_B^\infty x_t^4$ (second-order DC kinetics).

* To whom correspondence should be addressed

10.1021/ma980896g CCC: $18.00 © 1999 American Chemical Society
Published on Web 03/02/1999

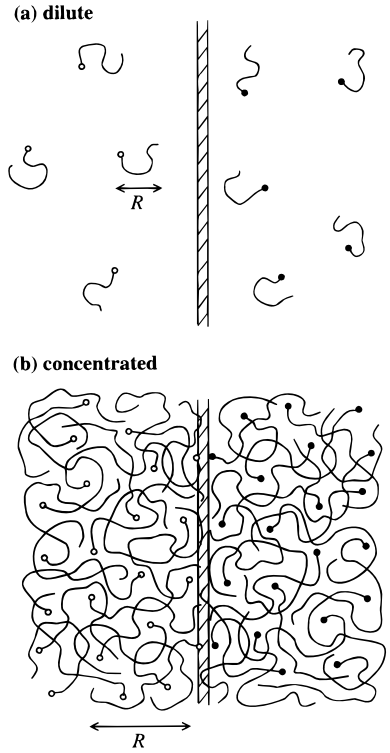

Figure 2. (a) Schematic of end-functionalized chains dilute in a background (not indicated) of unreactive but otherwise identical polymers. As shown, the densities of reactive ends are below the overlap threshold $1/R^3$. (b) Concentrated regime, with reactive group densities exceeding $1/R^3$.

employed in most reactive blending experiments are extremely small. A typical example is the reaction between carboxylic acid and epoxide ring groups[19] for which $Q_b t_a \approx 10^{-11}$. In addition, with the exception of ref 15, previous studies have been confined to reactive chains very dilute in an unreactive melt background (Figure 2a). Moreover, most of these works did not consider the reaction kinetics for all times. Generally, one expects[20] different kinetics before and after the longest polymer relaxation time τ. In ref 15 an attempt was made to develop kinetics for all times for the infinitely reactive case ($Q_b t_a = 1$). These authors found that for times sufficiently greater than τ the reaction rate is determined by center of gravity diffusion of polymer coils to the interface.

The objective of this paper is a systematic understanding of reaction kinetics, through all time regimes, as a function of local reactivity Q_b and bulk reactive group densities, n_A^∞ and n_B^∞ (see Figures 1 and 2). The densities may have any values in the range $0 < n_A^\infty \leq n_B^\infty \leq 1/(Na^3)$, where a is the size of reactive groups and the maximum allowed density corresponds to every chain end in the bulk being reactive. Generally, densities in either bulk are unequal, and our convention is always that the B side is the denser: $n_A^\infty \leq n_B^\infty$. We will establish four types of reaction kinetics and three distinct behaviors in the Q_b-n_B^∞ plane. Each of these three regions involves a different sequence of reaction kinetics regimes in time. We consider both unentangled and entangled polymer melts. For simplicity, effects associated with possible segregation of reactive groups to the interface are neglected here.[21]

Our analysis will be close to rigorous and adapts the general framework developed in ref 22 where interfacial

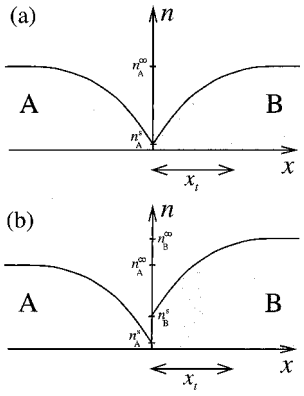

Figure 3. A reactant density depletion hole of size x_t grows at the interface for long times. (a) The symmetric case, $n_A^\infty = n_B^\infty$. The reactant density at the interface, n_A^s, tends asymptotically to zero. (b) The asymmetric case, $n_B^\infty > n_A^\infty$, where the interfacial density n_A^s on the dilute side tends to zero, while n_B^s approaches $n_B^\infty - n_A^\infty$ asymptotically.

reaction kinetics were studied for reactive species with a unique dynamical exponent, z, where

$$x_t = a\,(t/t_a)^{1/z} \tag{1}$$

is the rms displacement after time t. In order to apply this framework to reacting polymers, one has to deal with *several* consecutive dynamical regimes each with its own z value. For unentangled melts[23] the long time behavior is simple Fickian diffusion ($z = 2$), but at short times Rouse dynamics give $z = 4$. For entangled systems the successive dynamical regimes correspond to $z = 4$, 8, 4, 2.

For the remainder of the introduction let us review the main results of ref 22 for a single z value, using simple scaling arguments. Reactions are "switched on" at $t = 0$ and we seek the number of reactions per unit area, R_t, after time t, between molecular species A and B whose dynamics obey eq 1 for *all* times. The simplest imaginable behavior one might anticipate is "mean field" (MF) kinetics, i.e. that spatial distributions are unchanged from equilibrium; then the reaction rate, $\dot{R}_t \equiv dR_t/dt$, would be proportional to the equilibrium number of A−B reactive molecules in contact at the interface per unit area, $ha^3 n_A^\infty n_B^\infty$, multiplied by Q_b. Here h is the width of the interface (see Figure 1). This gives *second-order* kinetics, with a second-order rate constant $k^{(2)}$

$$\dot{R}_t = k^{(2)} n_A^\infty n_B^\infty, \quad k^{(2)} = Q_b h a^3 \quad \text{(MF kinetics)} \tag{2}$$

When are MF kinetics valid? Certainly, they are valid at very short times since equilibrium pertains at $t = 0$. However, at longer times the MF law cannot be valid since equilibrium is destroyed: eventually, in fact, a reactant density hole of size x_t develops close to the interface on the more *dilute* A side (see Figure 3). Consider an A group initially within x_t of the interface (see Figure 4) so that by time t diffusion will have brought it in contact with the interface. By time t it has collided with the interface of order $(t/t_a)(h/x_t)$ times. During each of these encounters, the probability that a B group is at the same location is $n_B^\infty a^3$. Hence the total reaction probability, $P_m(t) \approx (Q_b t_a)\,(n_B^\infty a^3)(t/t_a)(h/x_t) \sim$

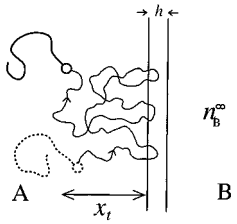

Figure 4. Meaning of the time scale t_m^*. Schematic of trajectory of an A reactive end group after time t, given the group was initially within diffusive range (x_t) of the interface. The number of encounters with the interface increases with a certain power of t. Thus even for relatively weakly reactive species, the A group is certain to have reacted with a B group in the other bulk after a sufficiently long time. This is the time scale t_m^*.

$t^{1-1/z}$, increases monotonically with t. Thus there exists a time scale t_m^* such that $P_m(t_m^*) = 1$

$$t_m^*/t_a = (Qt_a n_B^\infty a^3)^{-z/(z-1)}, \quad Q \equiv Q_b\, h/a \tag{3}$$

where the quantity Q emerges as an effective local reactivity, coarse-grained over the interface width h. For $t > t_m^*$, any A reactant within diffusional range of the interface will have reacted with the mean "reaction field" created by all of the B's. It follows that a depletion hole of size x_t develops on the A side and the reaction rate is limited by the diffusion of A's to the interface, $R_t \approx x_t n_A^\infty$. These kinetics are *first-order* diffusion controlled (labeled DC1) with a time-dependent first-order rate constant $k^{(1)}$:

$$\dot{R}_t = k^{(1)} n_A^\infty, \quad k^{(1)} \approx \frac{dx_t}{dt} \quad \text{(DC1 kinetics)} \tag{4}$$

Note that a similar reasoning applied to a B reactive group would yield a longer time scale than t_m^*. Hence the depletion hole develops on the more dilute A side first. In fact it was shown in ref 22 that the interfacial B density approaches the finite value $n_B^\infty - n_A^\infty$ for long times (see Figure 3).

These arguments tell us that MF theory is inapplicable for $t > t_m^*$. But is it valid for all times $t < t_m^*$? In fact nonequilibrium distributions may occur at shorter times in *two-body* correlation functions. Consider a pair of A−B groups which happened to be initially within diffusive range of each other (i.e. within x_t) at the interface. The number of times this pair collides by time t, N_{coll}, is of order the number of encounters the A makes with the interface, $(t/t_a)(h/x_t)$, multiplied by the probability it meets the B, a^3/x_t^3, during each of these encounters. Hence the total reaction probability $P_2(t) \approx Qt_a N_{coll} \sim t/x_t^4$ is increasing with time if x_t^4 increases more slowly than t, i.e. $z > 4$. This is similar to the situation arising in bulk reaction kinetics in d-dimensions, where different kinetics apply depending on whether x_t^d increases more rapidly ("noncompact" exploration) or more slowly ("compact" exploration) than t.[24] The interface problem is thus analogous to a 4-dimensional bulk system. Given this analogy, for the remainder of this paper we will refer to $z < 4$ and $z > 4$ interfacial systems as noncompact and compact, respectively.

In the noncompact case ($z < 4$) as time increases the fraction of pairs of the above type which succeed in reacting is becoming ever smaller. This suggests that pair correlations are weakly perturbed from equilibrium and MF kinetics apply for all $t < t_m^*$. The situation for $z > 4$ is very different. In this case there exists a characteristic two-body time scale, t_2^*, such that $P_2(t_2^*) = 1$

$$t_2^*/t_a = (Qt_a)^{-z/(z-4)} \quad (z > 4) \tag{5}$$

Now if it happens that Q and n_B^∞ are such that $t_2^* > t_m^*$, then this time scale is irrelevant since by t_2^* the reaction rate is already controlled by the diffusion of the dilute species to the interface. However if $t_2^* < t_m^*$, then after t_2^* any A−B pair which at $t = 0$ happened to be within diffusive range will have reacted by time t and a depletion hole will start growing in the two-body correlation function at the interface. The number of such pairs per unit area is $x_t^4 n_A^\infty n_B^\infty$ (see Figure 1), implying *second-order* diffusion controlled kinetics (or DC2) for $t > t_2^*$, with a time-dependent rate constant $k^{(2)}$

$$\dot{R}_t = k^{(2)} n_A^\infty n_B^\infty, \quad k^{(2)} \approx \frac{dx_t^4}{dt} \quad \text{(DC2 kinetics)} \tag{6}$$

These DC2 kinetics develop for $z > 4$ only. For how long do they persist? At first glance one might think until t_m^*; however, this is incorrect since the argument leading to t_m^* of eq 3 assumed equilibrium, whereas we have just seen that a hole of size x_t grows in the two-body density correlation function after time t_2^*. In fact the DC2 behavior continues until the time t_l, when a hole begins to grow in the density field itself, where

$$t_l/t_a \equiv (n_B^\infty a^3)^{-z/3} \tag{7}$$

is the diffusion time corresponding to the mean separation of B groups. After time t_l any A group initially closer than l to the interface, where $l \equiv (n_B^\infty)^{-1/3}$, will have had the chance to encounter a B group. Since reaction is certain for any pair within diffusive range (by definition of $t > t_2^*$) such a pair will definitely react. Thus, for $t > t_l$ almost every A reaching the interface will react, a depletion hole develops on the A side and reaction rates obey DC1 kinetics as in eq 4.

These arguments have led to three characteristic time scales which, we note, obey the relation $t_m^* = (t_2^*)^{1-\alpha} t_l^\alpha$ where $\alpha = 3/(z-1)$. This implies that the magnitude of t_m^* always lies between those of t_2^* and t_l. The condition $t_2^* = t_m^* = t_l$ defines a critical effective local reactivity, Q^*:

$$Q^* t_a \equiv (n_B^\infty a^3)^{(z-4)/3} \quad (z > 4) \tag{8}$$

There are two cases. (1) For "strongly" reactive systems, $Q > Q^*$ (or equivalently $t_2^* < t_m^* < t_l$), one has the following sequence of kinetic regimes: MF, DC2, DC1. (2) For "weakly" reactive systems, $Q < Q^*$ (or $t_l < t_m^* < t_2^*$), the sequence is as follows: MF, DC1. All of this is for $z > 4$ and should be contrasted with the $z < 4$ sequence: MF, DC1 (i.e. the same as the weak $z > 4$ case).

In the following sections we will see that for polymeric systems much of the above phenomenology is essentially unchanged and we will find a similar division of systems into "strong" and "weak". However, various new features appear such as a new type of MF kinetic behavior. Further, both Rouse and reptation dynamics exhibit marginal dynamical regimes, $z = 4$, for which we will find logarithmic corrections.

The paper is organized as follows. In Section II we derive a general expression for the reaction rate per unit area in Laplace space starting from the formalism of ref 22. Using the form of R_t from Section II, we identify in Section III four possible types of reaction kinetics (MF, DC2, DC1, MF^R) and three possible sequences of reaction kinetic types. The realized sequence depends on the values of Q and n_B^∞. In Sections IV and V we apply the general results of sections III and IV to unentangled and entangled melts, respectively. For each case we construct a "phase diagram" in the Q-n_B^∞ plane which completely describes the interfacial reaction kinetics. We conclude in Section V with a brief discussion.

II. General Expression for Reaction Rate

We consider A and B bulk phases occupying $x > 0$ and $x < 0$ respectively, with x being the direction orthogonal to the interface (see Figure 1). The A and B polymer species have the same degree of polymerization, N, and identical diffusive dynamics are assumed. We assume reaction products to be very dilute at the interface; in section V we analyze how their accumulation eventually diminishes reaction rates (excluded area effect).

Now reactions are "switched on" at $t = 0$. Then $\dot{R}_t$ is equal to the number of pairs of A−B reactive end-groups which are in contact per unit area at the interface, $ha^3 \rho_{AB}^s(t)$, multiplied by the local reactivity Q_b. Here, the two-body correlation function $\rho_{AB}^s(t)$ is the number of A−B reactive group pairs in contact at $x = 0$ per unit volume squared. Note translational invariance parallel to the interface dictates that $\rho_{AB}^s(t)$ is spatially uniform. Thus

$$\dot{R}_t = \lambda \rho_{AB}^s(t), \quad \lambda \equiv Q_b h a^3 = Q a^4 \tag{9}$$

where λ is a naturally occurring measure of reactive strength. In eq 9, we have implicitly taken the limit $h \to 0$; that is, our model can only be interpreted on scales large compared to h and t_h, the diffusion time corresponding to h.

In ref 22, where a general theory of interfacial reactions was developed, it was demonstrated that $\rho_{AB}^s(t)$ satisfies

$$\rho_{AB}^s(t) = n_A^\infty n_B^\infty - \lambda \int_0^t dt'\, S^{(4)}(t-t') \rho_{AB}^s(t') - \lambda n_B^\infty \int_0^t dt'\, S^{(1)}(t-t') \rho_{AB}^s(t') \tag{10}$$

where

$$S^{(1)}(t) \approx 1/x_t, \quad S^{(4)}(t) \approx 1/x_t^4 \tag{11}$$

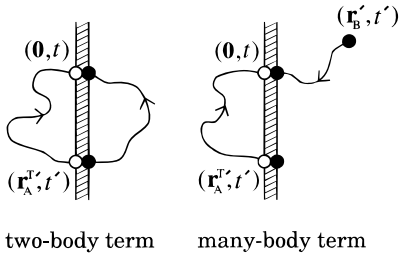

Figure 5. Schematic of the two sink terms on the left hand side of eq 10. The two-body term subtracts those A−B pairs which failed to reach the origin because both members reacted at an earlier time t' at point $\mathbf{r}_A^{T'}$. The many-body term subtracts those A−B pairs at the origin which failed to meet because *one* member of the pair reacted at an earlier time.

Here $S^{(4)}(t)$ is the return probability for an A−B *pair* of chain ends, i.e. the probability density that an A−B pair is in contact at time t at the interface, given it was in contact somewhere within the interface at $t = 0$. $S^{(1)}(t)$ is the corresponding return probability for a *single* chain end group (either A or B), namely the probability that a reactive end group initially within the interface returns to an interfacial site after time t.

The expression for the number of interfacial pairs of eq 10 can be understood physically as follows. Without reactions, this number would equal $n_A^\infty n_B^\infty$. Due to reactions, two terms must be subtracted off, as depicted in Figure 5. (1) The term involving $S^{(4)}$ subtracts off all pairs which would have recombined to meet at the interface at time t, but failed to do so because they reacted at the interface at a previous time t'. The weighting for such pairs is thus proportional to the probability a pair initially at the interface returns to the interface after a time $t - t'$, namely $S^{(4)}(t - t')$ (see Figure 5a). (2) The term involving $S^{(1)}$ subtracts off those pairs, at the interface at time t, only *one* member of which reacted at an earlier time t', say A. Consider the symmetric case $n_A^\infty = n_B^\infty$. Then the number of such pairs is proportional to the fraction of A members which return (the $S^{(1)}$ factor) multiplied by, roughly speaking, the density of B groups n_B^∞. In reality, the origin of this term is more complex; it involves three-body correlation functions as depicted in Figure 5b. In ref 22 this term was effectively closed in terms of ρ_{AB}^s after assuming certain simple physically motivated bounds on correlation functions.[25]

We remark that although the analysis in ref 22 was for a single dynamical regime, eq 10 is quite generally valid even for a sequence of different z values as in the present situation. In deriving eq 10, it has implicitly been assumed that polymer chain configurations are distributed as in equilibrium despite the occurrence of reactions.[20,26,27] This has allowed a closed relationship to be obtained in terms of those degrees of freedom describing the reactive end-groups only, whereas a proper treatment must first average out the locations of the other $N - 1$ monomers. There is considerable evidence from near-rigorous renormalization group analyses[28,29] that this approximation, which is standard in the field, correctly captures all scaling dependencies, though prefactors are unreliable.

The relation of eq 10 is a closed one for $\rho_{AB}^s(t)$. After Laplace transformation, $t \to E$, one can immediately solve for ρ_{AB}^s and obtain the reaction rate using eq 9.

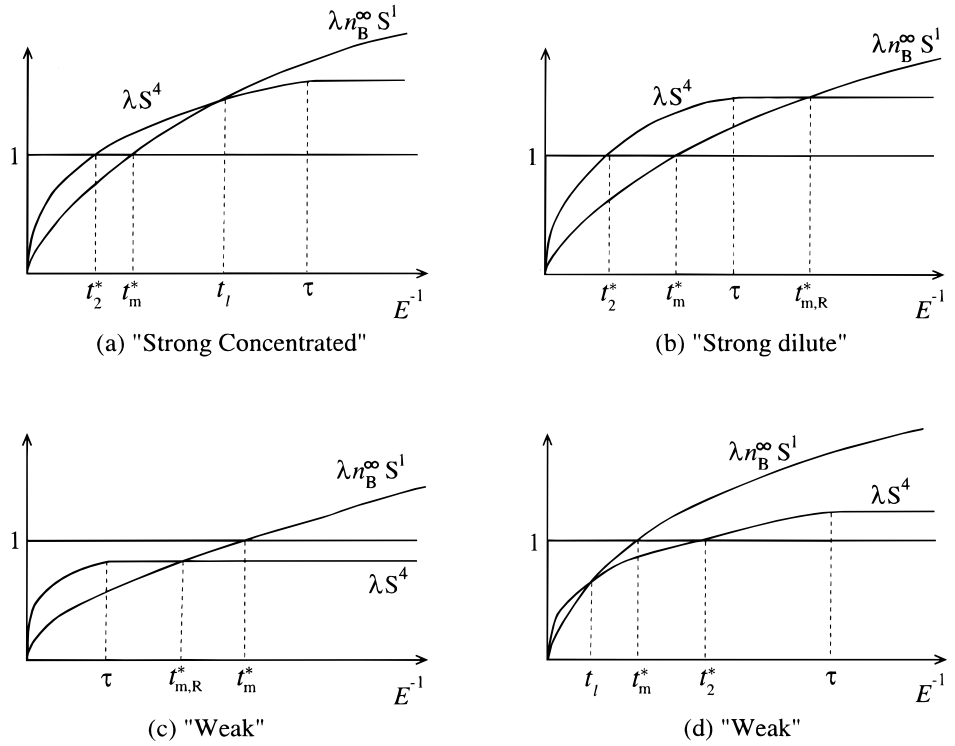

Figure 6. Schematic graphs of the three functions appearing in the denominator of the reaction rate $\dot{R}_t(E)$, eq 12, namely 1, $\lambda S^{(4)}(E)$, and $\lambda S^{(1)}(E)$. Using eqs A2, A4, B2, and B4 one can show that their most important features are the following: (1) $S^{(4)}$, $S^{(1)}$ tend to zero for $E^{-1} \to 0$. (2) As a function of E^{-1}, $S^{(1)}$ is monotonically increasing, while $S^{(4)}$ is initially increasing and saturates to its asymptotic value, $\int_0^\infty dt\, S^{(4)}(t)$ at $E^{-1} = \tau$. (3) $S^{(4)}$ and $S^{(1)}$ intersect once. Reaction kinetics are determined by the dominant of these three functions for each E value. Each intersection point defines a time scale. Diagrams a−d show the four possible sequences of dominant terms, as a function of E^{-1}, depending on the ordering of time scales determined by the values of λ (or Q) and n_B^∞. In case c, t_2^* is not defined since $\lambda S^{(4)}(E = 0)$ is less than unity.

This gives the following expression for the Laplace transform of the reaction rate per unit area, $\dot{R}_t(E)$:

$$\dot{R}_t(E) = \frac{\lambda n_A^\infty n_B^\infty}{E\,[1+ \lambda S^{(4)}(E) + \lambda n_B^\infty S^{(1)}(E)]} \qquad (12)$$

III. Four Types of Reaction Kinetics; Three Distinct Kinetic Sequences

The expression for the reaction rate, eq 12, involves the two return probabilities $S^{(1)}$ and $S^{(4)}$. Their forms depends on the detailed polymer dynamics. In Appendices A and B we present their explicit expressions for Rouse (unentangled melts) and reptation dynamics (entangled melts), respectively. We have then used these expressions to sketch the form of the three terms in the denominator of eq 12 in Figure 6, where parts a−d correspond to different values of chemical reactivity and n_B^∞, as we discuss below.

Now for a given E value, one of the 3 terms (namely 1, $\lambda S^{(4)}$, and $\lambda n_B^\infty S^{(1)}$) is dominant. This gives rise to different types of reaction kinetics as a function of time. In the region where the two terms involving $S^{(1)}$ and $S^{(4)}$ are much smaller than unity one recovers simple second-order MF kinetics, $\dot{R}_t(E) \approx \lambda n_A^\infty n_B^\infty/E$, implying

$$\dot{R}_t = k^{(2)} n_A^\infty n_B^\infty, \quad k^{(2)} \approx \lambda \equiv Q_b h a^3 \quad \text{(MF kinetics)} \qquad (13)$$

When the term involving $S^{(4)}$ is the dominant one, $\dot{R}_t(E) \approx n_A^\infty n_B^\infty/E S^{(4)}(E)$, leading to the second-order diffusion-controlled kinetics discussed in the introduction:

$$\dot{R}_t = k^{(2)} n_A^\infty n_B^\infty,$$
$$k^{(2)} \approx \begin{cases} \mathrm{d}x_t^4/\mathrm{d}t & (t < \tau) \ \text{(DC2 kinetics)} \\ 1/\int_0^\infty \mathrm{d}t' S^{(4)}(t') & (t > \tau) \ \text{(MF}^R \text{ kinetics)} \end{cases} \qquad (14)$$

In inverting the Laplace expression for the reaction rate we used the fact that the two-body interfacial return probability $S^{(4)}$, for values of the Laplace variable much *smaller* than the inverse coil relaxation time, tends to a constant value, $S^{(4)}(E \ll 1/\tau) \approx \int_0^\infty \mathrm{d}t\, S^{(4)}(t)$. This follows from eq 11 because the rms displacement $x_t \sim t^{1/2}$ for $t > \tau$. On the other hand, for E much *greater* than the inverse coil relaxation time, $S^{(4)}(E) \sim E^{4/z-1}$ since for times small compared to τ, $S^{(4)}(t) \approx 1/x_t^4 \sim t^{-4/z}$ with $z \geq 4$. In fact logarithmic corrections arise when $z = 4$ as occurs in both Rouse and reptation dynamics. These logarithmic corrections are evaluated in Appendix C.

Physically, the transition in eq 14 from a time-dependent rate constant at short times to a time-independent form at long times is similar to what occurs in diffusion-controlled polymer reaction kinetics in the *bulk*, reflecting the transition from compact exploration at short times to noncompact at long times.[24,30]

Finally, in regions where the $S^{(1)}$ term dominates, one recovers first-order diffusion-controlled kinetics, $\dot{R}_t(E) \approx n_A^\infty/E S^{(1)}(E)$, reflecting depletion of reactive

Table 1. Unentangled Chains: Characteristic Time Scales and Q^* [a]

	$t^{1/4}$ regime $t_h < t < \tau$	$t^{1/2}$ regime $t > \tau$
t_m^*	$t_a\,(Q\,t_a\phi_B)^{-4/3}$	$\tau[Q\,\tau(a/R)\phi_B]^{-2}$
t_2^*	$(t_h/e)e^{1/Qt_a}$	
t_l	$t_a\phi_B{}^{-4/3}[\ln(e\phi_B{}^{-4/3}t_a/t_h)]^{4/3}$	
$t_{m,R}^*$		$\tau[\ln(e\tau/t_h)/\phi_B(R/a)^3]^2$
t_{sat}		
$Q < Q^\dagger$		$1/(Q\phi_A\phi_B R/a)$
$Q > Q^\dagger$		$\tau/(N\phi_A)^2$
Q^*	$1/t_a\ln[e\phi_B{}^{-4/3}t_a/t_h]$	

[a] A given time scale has a different formula depending on whether it happens to be less than or greater than the Rouse time τ, or it may not exist (blank). $\phi_A \equiv n_A^\infty a^3$ denotes volume fraction of A reactive end groups (and similarly for ϕ_B). Expressions for t_{sat} are shown for $Q > Q^\dagger$ and $Q < Q^\dagger$, respectively (eq 23). Factors of e have been introduced for convenience, ensuring continuity of reaction rates.

Table 2. Unentangled Chains: Characteristic Time Scales and Q^* [a]

	$t^{1/4}$ regime $t_h < t < \tau$	$t^{1/2}$ regime $t > \tau$
t_m^*/t_a	$(\epsilon\phi_B)^{-4/3}$	$N^{-1}(\epsilon\phi_B)^{-2}$
t_2^*/t_a	$(h/a)^4e^{1/\epsilon}$	
t_l/t_a	$\phi_B{}^{-4/3}[\ln(\phi_B{}^{-4/3}a/h)]^{4/3}$	
$t_{m,R}^*/t_a$		$N^{-1}\phi_B{}^{-2}[\ln(N^2h/a)]^2$
t_{sat}/t_a		
$Q < Q^\dagger$		$1/(\epsilon\phi_A\phi_B N^{1/2})$
$Q > Q^\dagger$		$1/\phi_A{}^2$
Q^*t_a	$1/\ln(\phi_B{}^{-4/3}a/h)$	

[a] Identical with Table 1, but now with all quantities expressed in terms of $\epsilon \equiv Qt_a$ and molecular weight, N.

groups at the interface in the more dilute bulk:

$$\dot{R}_t = k^{(1)}n_A^\infty, \quad k^{(1)} \approx \frac{dx_t}{dt} \quad \text{(DC1 kinetics)} \qquad (15)$$

We used $S^{(1)} \sim E^{1/z-1}$, which follows from eq 11 and $x_t \sim t^{1/z}$.

Now at different times, so different terms will dominate the reaction rate of eq 12 and thus the reaction kinetics will be different. What is the realized sequence of kinetics in time? As one sees from Figure 6, this depends on the magnitude of chemical reactivity and the density of the more dense bulk. All possible cases are illustrated in parts a−d of Figures 6. These four cases correspond to different orderings of the time scales t_2^*, t_l, t_m^*, and $t_{m,R}^*$ of Figure 6. The time scales t_2^* and t_m^* are defined, respectively, by the intersection of the $S^{(4)}$ and the $S^{(1)}$ line with 1. Similarly, t_l and $t_{m,R}^*$ are defined by the intersection point of the $S^{(4)}$ and $S^{(1)}$ lines, depending on whether this intersection occurs at E greater or smaller than $1/\tau$. The explicit expressions for these time scales are summarized in Tables 1−4, constructed using the expressions for the return probabilities of appendices A and B.

In addition, we notice that the ordering of time scales t_2^*, t_m^*, and t_l in Figure 6a is the inverse of that in Figure 6d. These two diagrams thus become degenerate at $t_2^* = t_m^* = t_l$ in which case all three lines intersect at the same point. This condition defines a critical reactivity Q^*. Referring to Figure 6, one easily derives

$$t_l < t_m^* < t_2^* \quad (Q < Q^*), \quad t_2^* < t_m^* < t_l \quad (Q > Q^*) \qquad (16)$$

Let us now use Figure 6 and eqs 13−15 to derive all possible sequences of reaction kinetics. This defines three distinct regions in the $Q-n_B^\infty$ plane.

a. "Strong Concentrated." If a given experimental system belongs to the "strong concentrated" region (see Figures 7a(ii) and 8a(ii)), this corresponds to the situation shown in Figure 6a. Scanning from small E^{-1} to large E^{-1} (corresponding to scanning from small to large times) the reader can read off which of the three plotted curves is dominant for each time value. This

Table 3. Entangled Chains: Characteristic Time Scales and Q^* [a]

	unentangled Rouse $t^{1/4}$ $t_h < t < t_e$	breathing $t^{1/8}$ $t_e < t < t_b$	tube $t^{1/4}$ $t_b < t < \tau$	Fickian $t^{1/2}$ $t > \tau$
t_m^*	$t_a\,(Qt_a\phi_B)^{-4/3}$	$t_e[Qt_e(a/r_e)\phi_B]^{-8/7}$	$t_b[Qt_b(a/r_b)\phi_B]^{-4/3}$	$\tau[Q\tau(a/R)\phi_B]^{-2}$
t_2^*	$(t_h/e)e^{1/Qt_a}$	$t_e(Q\,t_a)^{-2}$	$(t_b/e)e^{1/[Q(a/r_b)^4t_b]}$	
t_l	$t_a\phi_B{}^{-4/3}[\ln(e\phi_B{}^{-4/3}t_a/t_h)]^{4/3}$	$t_e[\phi_B(r_e/a)^3]^{-8/3}$	$t_b[\phi_B(r_b/a)^3]^{-4/3}\{\ln[e(\phi_B r_b^3/a^3)^{-4/3}]\}^{4/3}$	
$t_{m,R}^*$				$\tau[\ln(e\tau/t_b)/\{\phi_B(R/a)^3\}]^2$
t_{sat}				
$Q < Q^\dagger$				$1/(Q\phi_A\phi_B R/a)$
$Q > Q^\dagger$				$\tau/(N\phi_A)^2$
Q^*	$1/t_a\ln[e\phi_B{}^{-4/3}t_a/t_h]$	$(1/t_a)[\phi_B(r_e/a)^3]^{4/3}$	$(r_b/a)^4/\{t_b\ln[e(\phi_B r_b^3/a^3)^{-4/3}]\}$	

[a] Similar to Tables 1 and 2 for the unentangled case, but now each time scale may arise in any of four dynamical regimes (apart from blank entries) with different definitions in each case.

Table 4. Entangled Chains: Characteristic Time Scales and Q^* [a]

	unentangled Rouse $t^{1/4}$ $t_h < t < t_e$	breathing $t^{1/8}$ $t_e < t < t_b$	tube $t^{1/4}$ $t_e < t < \tau$	Fickian $t^{1/2}$ $t > \tau$
t_m^*/t_a	$(\epsilon\phi_B)^{-4/3}$	$N_e{}^{2/7}(\epsilon\phi_B)^{-8/7}$	$N^{-1/3}N_e{}^{1/3}(\epsilon\phi_B)^{-4/3}$	$N_e(N\epsilon\phi_B)^{-2}$
t_2^*/t_a	$(h/a)^4e^{1/\epsilon}$	$N_e{}^2/\epsilon^2$	$N_e{}^2e^{N_e/(\epsilon N)}$	
t_l/t_a	$\phi_B{}^{-4/3}[\ln(\phi_B{}^{-4/3}a/h)]^{4/3}$	$\phi_B{}^{-8/3}N_e{}^{-2}$	$\phi_B{}^{-4/3}(NN_e)^{-1}[\ln(N/N_e^3)]^{4/3}$	
$t_{m,R}^*/t_a$				$N_e^{-1}[\ln(N/N_e)/\phi_B]$
t_{sat}/t_a				
$Q < Q^\dagger$				$1/(\epsilon\phi_A\phi_B N^{1/2})$
$Q > Q^\dagger$				$N/(N_e\phi_A^2)$
Q^*t_a	$1/\ln(\phi_B{}^{-4/3}a/h)$	$\phi_B{}^{4/3}N_e^2$	$N_e/[N\,\ln(\phi_B{}^{-4/3}(NN_e)^{-1})]$	

[a] As in Table 3, but now with all quantities expressed in terms of $\epsilon \equiv Qt_a$, the entanglement threshold N_e, and molecular weight, N.

leads to the following sequence of kinetics:

$$\mathrm{MF} \xrightarrow{t_2^*} \mathrm{DC2} \xrightarrow{t_l} \mathrm{DC1} \quad (Q > Q^*,\ t_l < \tau) \qquad (17)$$

Similarly, Figure 6b and Figure 6c/Figure 6d define two further regions.

b. "Strong Dilute."

$$\mathrm{MF} \xrightarrow{t_2^*} \mathrm{DC2} \xrightarrow{\tau} \mathrm{MF}^R \xrightarrow{t_{\mathrm{m,R}}^*} \mathrm{DC1} \quad (t_2^* < \tau,\ t_{\mathrm{m,R}}^* > \tau) \qquad (18)$$

c and d. "Weak."

$$\mathrm{MF} \xrightarrow{t_{\mathrm{m}}^*} \mathrm{DC1} \quad (t_{\mathrm{m}}^* < \tau,\ Q < Q^*, \text{ or } t_{\mathrm{m}}^* > \tau,\ t_2^* \text{ undefined}) \qquad (19)$$

Note that both parts c and d of Figure 6, having the same sequence of dominating terms, correspond to the same "weak" region.

IV. Unentangled Melts

A. Phase Diagram in $Q-n_{\mathrm{B}}^{\infty}$ Plane. In this section we apply the results of section III to melts of chains short enough to be unentangled: $N < N_{\mathrm{e}}$, where N_{e} is the entanglement threshold.[31] Polymer dynamics in such systems are well-described by Rouse dynamics (see Appendix A, eq A1), which are characterized by a dynamical exponent $z = 4$ for times less than $\tau \approx N^2 t_{\mathrm{a}}$, followed by $z = 2$ (Fickian diffusion) at long times. Thus interfacial kinetics are marginal and noncompact for $t < \tau$ and $t > \tau$, respectively (see discussion in Introduction).

First, by substitution of the Rouse expression for x_t in eqs 13−15, we derive explicit expressions for the reaction rate in each of the 4 possible kinetic regimes. The only complication is that the $z = 4$ regime is marginal, leading to logarithmic corrections during the DC2 regime. These corrections are evaluated in Appendix C. In addition, the time integral of $S^{(4)}$ in eq 14 has been evaluated in Appendix A (see eq A4). One thus has

$$\text{MF:} \qquad R_t \approx \lambda n_{\mathrm{A}}^{\infty} n_{\mathrm{B}}^{\infty}\, t$$

$$\text{DC2:} \qquad R_t \approx n_{\mathrm{A}}^{\infty} n_{\mathrm{B}}^{\infty} \{a^4/[t_{\mathrm{a}} \ln(e t/t_{\mathrm{h}})]\}\, t$$

$$\text{MF}^R\text{:} \qquad R_t \approx n_{\mathrm{A}}^{\infty} n_{\mathrm{B}}^{\infty} \{R^4/[\tau \ln(e\tau/t_{\mathrm{h}})]\}\, t$$

$$\text{DC1:} \qquad R_t \approx \begin{cases} n_{\mathrm{A}}^{\infty}\, a (t/t_{\mathrm{a}})^{1/4} & (t < \tau) \\ n_{\mathrm{A}}^{\infty}\, (Dt)^{1/2} & (t > \tau) \end{cases} \qquad (20)$$

Here $D \approx R^2/\tau$ denotes the long time self-diffusivity of a polymer chain and $R = N^{1/2} a$ is the unperturbed coil size.

Now depending on the values of the chemical reactivity and n_{B}^{∞}, the realized sequence in time of the kinetic regimes of eq 20 will be given by one of eqs 17−19. In Figure 7a(i) we have plotted the reactivity−density plane, where the lines $t_2^* = \tau$, $t_{\mathrm{m}}^* = \tau$, $t_l = \tau$, and $Q = Q^*$ have been drawn using their expression in Tables 1 and 2. Certain sections of these lines are omitted, in those regions where they are irrelevant (see below). These

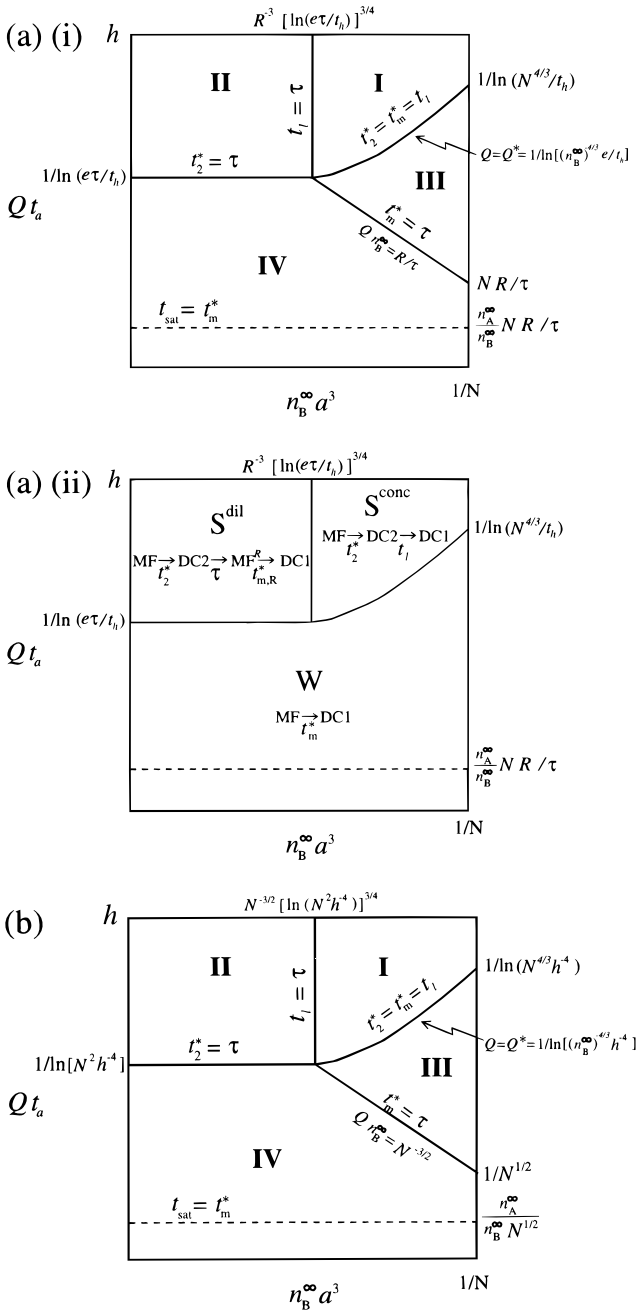

Figure 7. Interfacial reactions, unentangled melts, one reactive group per reactive polymer. "Phase diagram" of reaction kinetics as a function of renormalized reactivity $Q \equiv Q_{\mathrm{b}} h/a$ and density of the denser phase n_{B}^{∞}. Axes are logarithmic and units are chosen such that $t_a = a = 1$. Maximum possible density is $n_{\mathrm{B}}^{\infty} a^3 = 1/N$ (all chains functionalized). $\tau = N^2 t_a$ is the Rouse polymer relaxation time; all other time scales defined in tables 1 and 2. (a) (i) There are four regions in the phase diagram. The line $t_{\mathrm{sat}} = t_{\mathrm{m}}^*$ is shown for the special case of constant $n_{\mathrm{A}}^{\infty}/n_{\mathrm{B}}^{\infty}$ (note the convention, $n_{\mathrm{A}}^{\infty} \le n_{\mathrm{B}}^{\infty}$). (ii) Three types of kinetic behavior occur, in the three regions labeled S^{conc}, S^{dil}, and *W*. These symbols denote, respectively, "strong concentrated," "strong dilute" and "weak." In each region the sequence of kinetics is indicated. Below the $t_{\mathrm{sat}} = t_{\mathrm{m}}^*$ line interface saturation occurs before onset of the DC1 regime: kinetics are then always MF until saturation. (b) As in part a(i), but with reactivities and densities expressed in terms of molecular weight *N*.

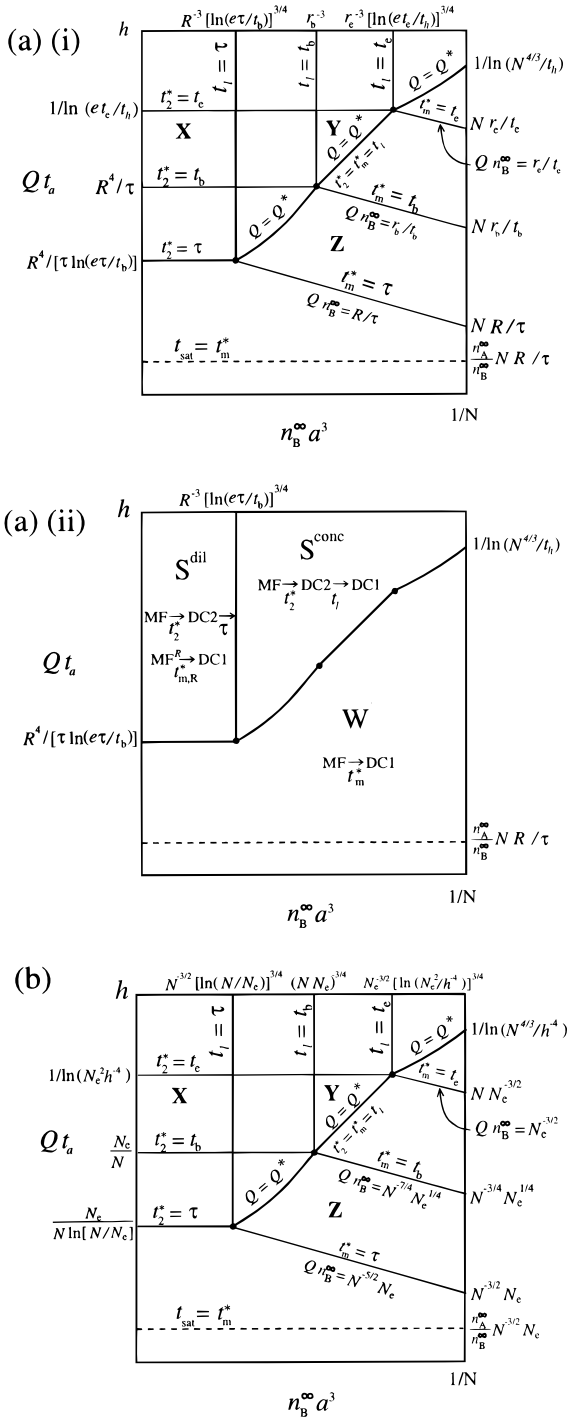

Figure 8. Phase diagram, as in Figure 7 but now for entangled melts. The longest relaxation time is now the reptation time $\tau = (N^3/N_e)t_a$; all other time scales defined in Tables 3 and 4. (a) (i) There are many more regions than in Figure 7a(i) for Rouse chains, since relevant time scales can now occur within any of four reptation regimes (see Tables 3 and 4). The $Q = Q^*$ line (defined by $t_2^* = t_m^* = t_l$) has three segments. Each segment has different dependencies on n_B^∞ as shown in Table 3. The line $t_{sat} = t_m^*$ is shown for constant n_A^∞/n_B^∞. (ii) The same three types of kinetic behavior occur as for unentangled systems, Figure 7a(ii). Below the $t_{sat} = t_m^*$ line there is again no DC1 regime. (b) As in part a(i), but with reactivities and densities expressed in terms of N and N_e.

lines define four distinct regions, indicated I−IV. Regions I and II are the "strong concentrated" and "strong dilute" regions, respectively, while region III plus region IV constitute the "weak" region. According to eqs 17−19, the kinetics in each region are as follows:

region I (strong concentrated):

$$\mathrm{MF} \xrightarrow{t_2^*} \mathrm{DC2} \xrightarrow{t_l} \mathrm{DC1} \xrightarrow{\tau} \mathrm{DC1}$$

region II (strong dilute):

$$\mathrm{MF} \xrightarrow{t_2^*} \mathrm{DC2} \xrightarrow{\tau} \mathrm{MF}^R \xrightarrow{t_{m,R}^*} \mathrm{DC1}$$

region III (weak): $$\mathrm{MF} \xrightarrow{t_m^*} \mathrm{DC1} \xrightarrow{\tau} \mathrm{DC1}$$

region IV (weak): $$\mathrm{MF} \xrightarrow{t_m^*} \mathrm{DC1} \qquad (21)$$

In the above, the notation DC1 $\xrightarrow{\tau}$ DC1 indicates that both the $t^{1/4}$ and $t^{1/2}$ DC1 kinetics of eq 20 are realized. Whenever DC1 appears just once, only the $t^{1/2}$ kinetics apply. Notice also that the weak region has two subregions, III and IV, depending on whether t_m^* happens to be smaller or greater than τ, respectively. Thus in region IV the $t^{1/4}$ DC1 regime is absent.

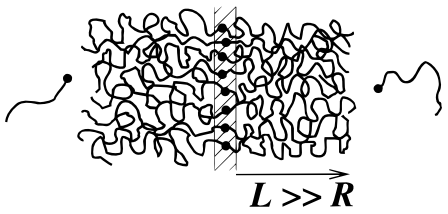

Figure 9. Reaction rates exponentially suppressed when the interface becomes crowded with diblock product at values of surface density above $1/N^{1/2}a^2$. This corresponds to the diblock brush being stretched, i.e., its size L being much bigger than the unperturbed chain dimension R.

B. Saturation of the Interface. So far the entire analysis has assumed the interface is unaltered by reaction products. This is valid at sufficiently short times. However, for end-functionalized chains, reactions generate an increasingly dense layer of A−B diblock copolymer product which beyond a certain time scale must inhibit further reactions (see Figure 9). Roughly speaking, at sufficiently high surface density, the diblock brush formed at the A−B interface becomes extended relative to the coil size R; when this happens the density of mobile bulk chains near the interface will drop significantly below the bulk values n_A^∞ and n_B^∞ with consequent[13] reduction in the reaction rate (see Figure 9).

It can been shown[32−35] that the surface density at which such diblocks start to feel one another laterally, and therefore become stretched, is one diblock per interface area $N^{1/2}a^2$. This is simple to understand if one notes that an imaginary plane slicing through an unperturbed bulk polymer melt is intersected by one chain per area $N^{1/2}a^2$, since there are R/Na^3 chains per unit area of such a surface which are close enough, i.e. within distance $R = N^{1/2}a$, to intersect it (the volume of one chain is Na^3). Hence any attempt to load a surface beyond this areal density must perturb the chains relative to their Gaussian dimensions in a free melt: the chains cannot fit into space unless they stretch. According to a detailed analysis in ref 13, the rate constant is

exponentially suppressed for diblock surface densities ρ_{surf} above this critical level

$$k \sim \exp(-9Na^4\rho_{surf}{}^2), \quad \rho_{surf} > 1/N^{1/2}a^2 \qquad (22)$$

It follows that for very large $N \gg 1$, reactions essentially cease at a time t_{sat} where $R_{t_{sat}} = 1/N^{1/2}a^2$. In Appendix D we show that t_{sat} is always greater than τ and given by

$$t_{sat} = \begin{cases} 1/[Qa^5Rn_A^\infty n_B^\infty] & (t_{sat} < t_m^*,\ Q < Q^\dagger) \\ \tau/(Nn_A^\infty a^3)^2 & (t_{sat} > t_m^*,\ Q > Q^\dagger) \end{cases} \qquad (23)$$

Recall that t_m^* is a decreasing function of Q at fixed n_B^∞ (see Table 1). At the boundary between the two cases in eq 23, Q has the value $Q^\dagger$ given below:

$$t_{sat} = t_m^*, \quad Qt_a = Q^\dagger t_a \equiv \frac{n_A^\infty}{n_B^\infty} N\frac{R}{a}\frac{t_a}{\tau} \qquad (24)$$

The line $Q = Q^\dagger$ is indicated in the phase diagrams of Figure 7. Below this line, saturation of the interface at time t_{sat} truncates the $t > \tau$ MF regime before the final DC1 kinetics can be realized. Above it, saturation occurs after the onset of DC1 kinetics and the full "weak" sequence is realized.

V. Entangled Melts

When both bulks contain very long chains, $N > N_e$, dynamics are strongly influenced by entanglements.[31] Our framework is the reptation model,[23,36] briefly stated in Appendix B. Three dynamical regimes occur for times less than the longest polymer relaxation time, the reptation time $\tau = (N^3/N_e)t_a$. In chronological order, x_t varies as $t^{1/4}$, $t^{1/8}$, and $t^{1/4}$. These are respectively marginal, compact and marginal regimes. The long times behavior is again simple center of gravity diffusion, $x_t \sim t^{1/2}$, as for Rouse dynamics.

Repeating the procedure of the previous section, but now using the reptation dynamics of eq B1, one obtains the time scales listed in Tables 3 and 4 and the phase diagram shown in Figure 8a(ii) and Figure 8b. Compared to unentangled kinetics, there are now many more sub-regions, corresponding to the increased number of dynamical regimes. Once again, however, there are only three distinct regions in terms of the sequence of kinetics. The discussion of saturation effects at the interface is identical to that for unentangled systems; t_{sat} is again given by eq 23, with τ understood as the reptation time. Similar remarks apply to $Q^\dagger$ of eq 24.

Examples. Consider, for example, the three points X, Y, and Z marked in the $Q-n_B^\infty$ plane in parts a(i) and b of Figure 8. Point X belongs to the strong dilute region, where the relevant time scales are t_2^* and $t_{m,R}^*$. Moreover, its location tells us that $t_e < t_2^* < t_b$. Thus R_t is given by

$$R_t \approx \begin{cases} \lambda n_A^\infty n_B^\infty\, t & (t < t_2^*, \text{MF}) \\ n_A^\infty n_B^\infty\, r_e^4\,(t/t_e)^{1/2} & (t_2^* < t < t_b, \text{DC2}) \\ n_A^\infty n_B^\infty\, r_b^4\,(t/t_b)/\ln(et/t_b) & (t_b < t < \tau, \text{DC2}) \\ n_A^\infty n_B^\infty\, R^4\,(t/\tau)/\ln(e\tau/t_b) & (\tau < t < t_{m,R}^*, \text{MF}^R) \\ n_A^\infty\,(Dt)^{1/2} & (t_{m,R}^* < t < t_{sat}, \text{DC1}) \end{cases} \quad \text{(point } X\text{)} \qquad (25)$$

Now consider point Y, belonging to the strong concentrated class. Its Q value is the same as that of point X, and hence t_2^* is the same, $t_e < t_2^* < t_b$. However since n_B^∞ is greater, the crossover time to DC1 kinetics is smaller; in the strong concentrated region this occurs at t_l. The location of Y implies $t_e < t_l < t_b$. Thus

$$R_t \approx \begin{cases} \lambda n_A^\infty n_B^\infty\, t & (t < t_2^*, \text{MF}) \\ n_A^\infty n_B^\infty\, r_e^4\,(t/t_e)^{1/2} & (t_2^* < t < t_l, \text{DC2}) \\ n_A^\infty\, r_e\,(t/t_e)^{1/8} & (t_l < t < t_b, \text{DC1}) \\ n_A^\infty r_b\,(t/t_b)^{1/4} & (t_b < t < \tau, \text{DC1}) \\ n_A^\infty\,(Dt)^{1/2} & (\tau < t < t_{sat}, \text{DC1}) \end{cases} \quad \text{(point } Y\text{)} \qquad (26)$$

In this case there are three phases to the DC1 regime, each with a different power law in time. The breathing modes phase introduces a $t^{1/8}$ law which has no parallel in the unentangled case.

Finally, the point Z has the same n_B^∞ value as Y, but the reactivity is so much lower that $Q < Q^*$ and the DC2 regime vanishes: Z now belongs to the weak region where the relevant time scale is t_m^*, and its specific location tells us that $t_b < t_m^* < \tau$. Thus

$$R_t \approx \begin{cases} \lambda n_A^\infty n_B^\infty\, t & (t < t_m^*, \text{MF}) \\ n_A^\infty\, r_b\,(t/t_b)^{1/4} & (t_m^* < t < \tau, \text{DC1}) \\ n_A^\infty\,(Dt)^{1/2} & (\tau < t < t_{sat}, \text{DC1}) \end{cases} \quad \text{(point } Z\text{)} \qquad (27)$$

VI. Summary

Since the results of this work are rather involved, we present below a brief summary of our main findings.

1. Short Times, Second-Order Kinetics: $R_t = k^{(2)}n_A^\infty n_B^\infty$. Initially, reaction kinetics are always second order. At the shortest times, simple mean field (MF) kinetics apply since spatial distributions of reactive groups are undisturbed from equilibrium. The second-order rate constant $k^{(2)}$ is then independent of time, and the number of reactions per unit area grows linearly in time, $R_t \approx Qa^4\, n_A^\infty n_B^\infty\, t$.

After this MF phase, there are two possibilities. A direct transition to first-order kinetics may occur. However, if the functional groups are very reactive then a second-order diffusion-controlled (DC) regime will onset. During this regime, any A−B reactive pair will definitely react if close enough to meet through diffusion; i.e., if the pair separation was initially less than x_t, the rms distance diffused after time t. The time dependence of these kinetics, which we called DC2, is rather peculiar: $R_t \approx x_t{}^4 n_A^\infty n_B^\infty$.

These DC2 kinetics can only occur if space is explored by the reactive groups in a sufficiently "compact" manner: the requirement is that $x_t{}^4$ must grow less rapidly than t, or else as t (marginal case). This means that the long time $t^{1/2}$ Fickian diffusion regime can never involve DC2 kinetics. On the other hand, given the $t^{1/4}$ and $t^{1/8}$ short time laws of polymer melt dynamics, DC2 regimes will occur for times less than τ, the longest polymer relaxation time, provided Q is large enough. These are the upper regions denoted S^{conc} and S^{dil} in the phase diagrams of Figures 7 and 8, in the $Q-n_B^\infty$ plane.

Thus, time dependencies during these short time DC2 regimes are as follows. For unentangled chains ($x_t \sim t^{1/4}$)

we obtained $R_t \sim t/(\ln t)$, logarithmic corrections arising in this marginal case. For entangled chains $R_t \sim t/(\ln t)$ again during the two $t^{1/4}$ regimes, while $R_t \sim t^{1/2}$ for the $t^{1/8}$ regime (the breathing modes).

There is a complication to this picture for dilute but highly reactive systems: in such cases, before the first-order regime onsets a reentrant second-order MF regime is realized after the DC2 regime. This behavior, occurring in region S^{dil} in Figures 7 and 8, was the subject of earlier theoretical studies.[12−14] However, these works did not consider the final first-order regime.

2. Long Times, First-Order Kinetics: $R_t \approx x_t n_A^\infty$). At a certain time scale, kinetics become first order. These kinetics are always diffusion-controlled (DC) and always have the same structure, $R_t \approx x_t n_A^\infty$. We called them DC1. They onset when the reaction rate becomes controlled by the diffusion of the more dilute A reactive species to the interface.

An important issue is whether or not DC1 kinetics onset before τ. This requires sufficiently large Q and that the reactive groups be on average closer to the interface than their coil size R; that is, n_B^∞ must exceed the coil overlap threshold, $n_B^\infty > 1/R^3$. These conditions are satisfied in the sum of the region S^{conc} and that part of region W for which $t_m^* < \tau$. In this portion of the phase plane, a series of short time regimes occur: $R_t \sim t^{1/4}$ for unentangled chains, while for entangled systems, in chronological order $R_t \sim t^{1/4}$, $R_t \sim t^{1/8}$, and $R_t \sim t^{1/4}$ may occur, depending on Q, n_B^∞. In all cases, whether DC1 behavior onsets before or after τ, the long time behavior corresponds to the Fickian center of gravity diffusion, $R_t \sim t^{1/2}$.

3. Saturation. The accumulating copolymer product ultimately saturates the interface after time t_{sat}. (We do not discuss here interesting effects such as interface destabilization due to surface tension reduction by copolymer product; in some cases this appears to perpetuate reactions by generating new surface area.) If $Q < Q^\dagger$, then saturation occurs before the final first order DC kinetics regime has begun. For such cases, kinetics are always MF.

A dimensionless measure of reactive strength is $Q_b t_a$, where t_a is the monomer relaxation time. For "ordinary" chemical species,[37−39] one has $Q_b t_a \lesssim 10^{-6}$. Then for unentangled chains of maximum possible length,[31] $N \approx 300$, eq 24 implies $Q^\dagger t_a \approx 0.06$, which is many orders of magnitude higher than typical values of Qt_a. Thus kinetics are always MF until saturation at t_{sat}. Considering maximum reactant densities, we obtain $t_{sat} \gtrsim 6 \times 10^4\, \tau \approx 0.5$ s for $N = 300$. In the case of entangled melts with, e.g., $N = 10^4$, $Q^\dagger t_a \approx 10^{-4}$. Thus even here MF kinetics are likely to apply up to t_{sat}. For $N = 10^4$, $N_e \approx 300$, and maximum densities, the saturation time $t_{sat} > 10^4 \tau \approx 3 \times 10^3$ s.

For radicals,[37−40] on the other hand, $Q_b t_a \approx 1$. Such systems are located in the S^{conc} or S^{dil} regions and the full sequence of regimes is realized well before saturation. The value of t_{sat} then depends only on n_A^∞ and ranges from τ at maximum density to arbitrarily large values as density decreases.

4. Experimental Outlook. At present there is very little experiment, either numerical[16] or real, to compare theory with. Some indirect qualitative information is available from reactive blending studies where data suggest MF kinetics. For example, in ref 8, varying amounts of coupling agent were added, corresponding in effect to different values of Q. The higher Q, the more copolymers were formed at a given time, as inferred from smaller droplet sizes of the minority phase. MF kinetics are suggested, since reaction rates in all DC regimes are independent of Q.

Also potentially relevant are studies where fracture toughness is measured after conducting interface-reinforcing polymer reactions for different periods of time.[1−3,41,42] This allows inference of time dependence of the copolymer product surface coverage if one knows how the latter is related to fracture toughness. Unfortunately, the latter is itself a complex issue, and frequently the polymers involved are multifunctionalized and one phase is sometimes cross-linked or glassy. If one makes the assumption that for low copolymer surface coverage the increase in fracture toughness is proportional to the surface density of copolymer grafts, then the measurements of ref 2 imply a linear increase in the number of reactions with time, again consistent with simple MF kinetics.

Basic experiments measuring reaction kinetics in the $Q_b - n_B^\infty$ plane are badly needed. Since diffusion-controlled behavior requires highly reactive chemical groups, the most interesting parts of our predicted phase diagrams can be probed only by radical species or else by photophysical methods. Radicals have also been used in some recent reactive blending systems.[43] As experimental probes, radicals have many advantages. For example, their lifetimes can be made extremely long by suitable choice of medium, such that only radical−radical recombinations contribute significantly to their decay. Novel experiments generating chains with radical end groups near interfaces hold the promise of experimentally testing many of the predictions contained in this work.

Acknowledgment. This work was supported by the National Science Foundation under Grant No. DMR-9403566. We thank Uday Sawhney for stimulating discussions.

Appendix A. Rouse Model: Dynamics and Return Probabilities

The dynamics of polymers in an unentangled melt are well known to obey Rouse dynamics.[23,36,31] The Rouse model leads to the following results:

$$x_t \approx \begin{cases} a\,(t/t_a)^{1/4} & (t < \tau) \\ R\,(t/\tau)^{1/2} & (t > \tau) \end{cases} \quad \frac{\tau}{t_a} = N^2, \quad \frac{R}{a} = N^{1/2} \tag{A1}$$

Here τ is the longest polymer relaxation time. Thus Rouse dynamics are characterized by two dynamical exponents: $z = 4$ for $t < \tau$ and $z = 2$ for $t > \tau$. In the context of interfacial reaction kinetics, an early marginal regime ($z = 4$) is followed by a noncompact one ($z = 2$). This last regime is simple Fickian diffusion.

From eq 11 and using x_t as defined in eq A1, one obtains

$$S^{(1)}(E) \approx \begin{cases} (t_a/a)\,(Et_a)^{-3/4} & (E^{-1} < \tau) \\ (\tau/R)\,(E\tau)^{-1/2} & (E^{-1} > \tau) \end{cases} \tag{A2}$$

while eqs 11 and eq A1 lead to the following approximate expression for $S^{(4)}$:

$$S^{(4)}(E) \approx \int_{t_h}^{\tau} dt' \, e^{-Et'} \frac{1}{a^4} \frac{t_a}{t'} + \int_{\tau}^{\infty} dt' \, e^{-Et'} \frac{1}{R^4} \left(\frac{\tau}{t'}\right)^2 \quad \text{(A3)}$$

We have introduced a cut-off at t_h. (At shorter times kinetics are as for a standard bulk reaction problem, with $S^{(4)} \approx 1/(hx_t^3)$; one can show that the $t < t_h$ contribution[22] is of the same order as that from the lower limit $t = t_h$ in eq A3.) For $E\tau > 1$ the first integral dominates and one can set its upper limit to infinity with small error. Thus

$$S^{(4)}(E) \approx \begin{cases} (t_a/a^4) \ln(1/Et_h) & (E^{-1} < \tau) \\ \int_0^{\infty} dt \; S^{(4)}(t) \approx (t_a/a^4) \ln(\tau/t_h) & (E^{-1} > \tau) \end{cases} \quad \text{(A4)}$$

Appendix B. Reptation Model: Dynamics and Return Probabilities

In this appendix we briefly review the reptation model,[23,36] describing the entanglement-dominated motion of long chains, $N > N_e$, where N_e is the entanglement threshold. This model treats entanglements as inhibiting lateral chain motion on a certain scale r_e corresponding to a portion of chain comprising N_e units: in effect, each chain is confined to a "tube" of diameter $r_e = N_e^{1/2}a$. We assume the tube diameter exceeds the interface width h. For times shorter than the diffusion time $t_e = N_e^2 t_a$ corresponding to r_e, monomers do not feel the tube and obey Rouse-like dynamics ($z = 4$) as in unentangled melts. For $t > t_e$, the chain diffuses curvilinearly up and down the tube in one-dimensional $t^{1/4}$ Rouse motion. These are the "breathing modes." The monomer rms displacement in space increases as $t^{1/8}$, since the tube is itself a random walk. This regime continues until $t_b = N^2 t_a$, corresponding to a monomer diffusion distance $r_b = r_e(N/N_e)^{1/4}$, by which time the chain has relaxed its configuration relative to the tube. For longer times the chain diffuses coherently along the tube and monomer rms displacement is $t^{1/4}$. This "tube diffusion" regime persists until the longest polymer relaxation or "reptation" time, $\tau = (R/r_b)^4 t_b = (N^3/N_e)t_a$, by which time the chain has completely diffused out of its initial tube into a new and uncorrelated one. Here $R = N^{1/2}a$ is the rms coil size. The process then repeats itself indefinitely, corresponding to long time Fickian center of gravity motion, $x_t = R(t/\tau)^{1/2}$. In summary

$$x_t \approx \begin{cases} a\,(t/t_a)^{1/4} & (t < t_e \equiv N_e^2 t_a, \text{ "Rouse"}) \\ r_e\,(t/t_e)^{1/8} & (t_e < t < t_b \equiv N^2 t_a, \text{ "breathing"}) \\ r_b\,(t/t_b)^{1/4} & (t_b < t < \tau \equiv (R/r_b)^4 = N^3 t_a/N_e, \text{ "tube"}) \\ R\,(t/\tau)^{1/2} & (t > \tau, \text{ "Fickian"}) \end{cases} \quad \text{(B1)}$$

Thus, there are four regimes with the following sequence of dynamical exponents: $z = 4, 8, 4, 2$. Two of these regimes are marginal (occurring at small times $t < \tau$), and one is noncompact (long times, $t > \tau$).

The Laplace transform of $S^{(1)}(t) \approx 1/x_t$ in eq 11 is then evaluated using eq B1, which gives

$$S^{(1)}(E) \approx \begin{cases} (t_a/a)\,(Et_a)^{-3/4} & (t_a < E^{-1} < t_e) \\ (t_e/r_e)\,(Et_e)^{-7/8} & (t_e < E^{-1} < t_b) \\ (t_b/r_b)\,(Et_b)^{-3/4} & (t_b < E^{-1} < \tau) \\ (\tau/R)\,(E\tau)^{-1/2} & (\tau < E^{-1}) \end{cases} \quad \text{(B2)}$$

Similarly $S^{(4)}(t) \approx 1/x_t^4$ (eq 11) is calculated using eq B1. Its Laplace transform is approximately given by

$$S^{(4)}(E) \approx \int_{t_h}^{t_e} dt' \, e^{-Et'} \frac{1}{a^4} \frac{t_a}{t'} + \int_{t_e}^{t_b} dt' \, e^{-Et'} \frac{1}{r_e^4} \left(\frac{t_e}{t'}\right)^{1/2} + \int_{t_b}^{\tau} dt' \, e^{-Et'} \frac{1}{r_b^4} \frac{t_b}{t'} + \int_{\tau}^{\infty} dt' \, e^{-Et'} \frac{1}{R^4} \left(\frac{\tau}{t'}\right)^2 \quad \text{(B3)}$$

We have introduced a cutoff in the Laplace transform integral at $t_h = t_a(h/a)^4$ using the same reasoning as in Rouse dynamics (see eq A3). This leads to

$$S^{(4)}(E) \approx \begin{cases} (t_a/a^4) \ln(1/Et_h) & (t_h < E^{-1} < t_e) \\ (t_e/r_e^4)\,(Et_e)^{-1/2} & (t_e < E^{-1} < t_b) \\ (t_b/r_b^4) \ln(1/Et_b) & (t_b < E^{-1} < \tau) \\ \int_0^{\infty} dt \; S^{(4)}(t) \approx (\tau/R^4) \ln(\tau/t_b) & (\tau < E^{-1}) \end{cases} \quad \text{(B4)}$$

Appendix C. Marginal Regimes ($z = 4$): Logarithmic Corrections to DC2 Kinetics

In this appendix we derive the form of DC2 kinetics in marginal regimes, starting from the general expression for DC2 kinetics in Laplace space, $\dot{R}_t(E) = n_A^{\infty} n_B^{\infty}/ES^{(4)}(E)$ (see discussion following eq 14). Consider first the short time marginal $t^{1/4}$ regime of Rouse dynamics. Inserting $S^{(4)}(E)$ for $E^{-1} < \tau$ from eq A4 in $\dot{R}_t(E)$ and Laplace inverting, one has

$$\dot{R}_t = k^{(2)} n_A^{\infty} n_B^{\infty}, \quad k^{(2)} \approx a^4/[t_a \ln(et/t_h)] \quad (t_h < t < \tau) \quad \text{(DC2 kinetics, Rouse)} \quad \text{(C1)}$$

(for details on the inverse Laplace transform of $1/[E \ln(1/Et_h)]$ the reader is referred to ref 22). Similarly, for reptation dynamics, inserting $S^{(4)}(E)$ from eq B2 in $\dot{R}_t(E)$ gives for the two short time marginal regimes

$$\dot{R}_t = k^{(2)} n_A^{\infty} n_B^{\infty}, \quad k^{(2)} \approx \begin{cases} a^4/[t_a \ln(et/t_h)] & (t_h < t < t_e) \\ r_b^4/[t_b \ln(et/t_b)] & (t_b < t < \tau) \end{cases} \quad \text{(DC2 kinetics, reptation)} \quad \text{(C2)}$$

In the above expressions, it has been convenient to introduce factors of e in the logarithms to ensure continuity of reaction rates.

Appendix D. Evaluation of t_{sat}

Note first that t_{sat} must exceed τ; even at the maximum density, $n_A^{\infty} = 1/Na^3$, and even if reactions were diffusion-controlled, a time τ would be required to react all those chains with ends within R of the interface and thereby saturate it. Note also that under MF^R kinetics, to within a logarithmic prefactor, $R_t \approx (n_A^{\infty}/n_B^{\infty})/R^2$ at $t = t_{m,R}^*$ (see eq 20). Since this surface density is less than

$1/N^{1/2}a^2$, hence $t_{sat} > t^*_{m,R}$. It follows that at the time t_{sat}, reaction kinetics are either MF or DC1 (see eqs 17−19). Using the $t > \tau$ expressions for R_t implied by eqs 20 and 21 and equating these to $R_{t_{sat}}$, one obtains eq 23.

References and Notes

(1) Boucher, E.; Folkers, J. P.; Hervert, H.; Léger, L.; Creton, C. *Macromolecules* **1996**, *29*, 774.
(2) Beck Tan, N. C.; Tai, S.-K.; Briber, R. M. *Polymer* **1996**, *37*, 3509−3519.
(3) Tan, N. C. B.; Peiffer, D. G.; Briber, R. M. *Macromolecules* **1996**, *29*, 4969−4975.
(4) Scott, C.; Macosko, C. *J. Polym. Sci.: Part B* **1994**, *32*, 205−213.
(5) Creton, C.; Kramer, E. J.; Hui, C. Y.; Brown, H. R. *Macromolecules* **1992**, *25*, 3075−3088.
(6) Washiyama, J.; Creton, C.; Kramer, E. J.; Xiao, F.; Hui, C. Y. *Macromolecules* **1993**, *25*, 6011−6020.
(7) Gersappe, D.; Irvine, D.; Balazs, A. C.; Liu, Y.; Sokolov, J.; Rafailovich, M.; Schwarz, S.; Peiffer, D. G. *Science* **1994**, *265*, 1072−1074.
(8) Okamoto, M.; Inoue, T. *Polym. Eng. Sci.* **1993**, *33*, 175−182.
(9) Sundararaj, U.; Macosko, C. *Macromolecules* **1995**, *28*, 2647−2657.
(10) Milner, S. T.; Xi, H. *J. Rheol.* **1996**, *40*, 663.
(11) Orr, C. A.; Adedeji, A.; Hirao, A.; Bates, F. S.; Macosko, C. W. *Macromolecules* **1997**, *30*, 1243.
(12) O'Shaughnessy, B.; Sawhney, U. *Phys. Rev. Lett.* **1996**, *76*, 3444−3447.
(13) O'Shaughnessy, B.; Sawhney, U. *Macromolecules* **1996**, *29*, 7230−7239.
(14) Fredrickson, G. H. *Phys. Rev. Lett.* **1996**, *76*, 3440−3443.
(15) Fredrickson, G. H.; Milner, S. T. *Macromolecules* **1996**, *29*, 7386−7390.
(16) Muller, M. *Macromolecules* **1997**, *30*, 6353−6357.
(17) Mita, I.; Horie, K. *J. Macromol. Sci., Rev. Macromol. Chem. Phys.* **1987**, *C27* (1), 91−169.
(18) Wisnudel, M. D.; Torkelson, J. M. *J. Polym. Sci., Polym. Phys. Ed.* **1996**, *34*, 2999.
(19) Guégan, P.; Macosko, C. W.; Ishizone, T.; Hirao, A.; Nakahama, S. *Macromolecules* **1994**, *27*, 4993−4997.
(20) Friedman, B.; O'Shaughnessy, B. *Int. J. Mod. Phys. B* **1994**, *8*, 2555−2591.
(21) de Gennes, P. G. *C. R. Acad. Sci.* **1988**, *307 II*, 1841.
(22) O'Shaughnessy B.; Vavylonis D. http://xxx.lanl.gov/abs/cond-mat/9807110, to appear in *Eur. Phys. J. B.*
(23) Doi, M.; Edwards, S. F. *The Theory of Polymer Dynamics*; Clarendon Press: Oxford, England, 1986.
(24) de Gennes, P. G. *J. Chem. Phys.* **1982**, *76*, 3316−3321, 3322−3326.
(25) In fact the $S^{(1)}$ term as it appears in eq 12 is correct only for sufficiently long times; the proper expression includes an extra time-dependent prefactor of order unity. It turns out, however, that this term is only relevant at long times, where the displayed form is valid.[22]
(26) O'Shaughnessy, B. *J. Chem. Phys.* **1991**, *94*, 4042−4054.
(27) O'Shaughnessy, B. *Phys. Rev. Lett.* **1993**, *71*, 3331; *Macromolecules* **1994**, *27*, 3875.
(28) Friedman, B.; O'Shaughnessy, B. *Phys. Rev. Lett.* **1988**, *60*, 64−67.
(29) Friedman, B.; O'Shaughnessy, B. *Europhys. Lett.* **1993**, *23*, 667; *Macromolecules* **1993**, *26*, 5726.
(30) O'Shaughnessy, B.; Vavylonis, D. *Eur. Phys. J. B* **1998**, *6*, 363−372.
(31) Ferry, J. D. *Viscoelastic Properties of Polymers*, 3rd ed.; John Wiley and Sons: New York, 1980.
(32) Zhulina, E. B.; Borisov, O. V.; Brombacher, L. *Macromolecules* **1991**, *24*, 4679−4690.
(33) Zhulina, E. B.; Borisov, O. V. *J. Colloid Interface Sci.* **1991**, *144*, 507−520.
(34) Semenov, A. N. *Sov. Phys. JETP* **1985**, *61*, 733.
(35) Semenov, A. N. *Macromolecules* **1992**, *25*, 4967.
(36) de Gennes, P. G. *Scaling Concepts in Polymer Physics*; Cornell Univ. Press: Ithaca, NY, 1985.
(37) Denisov, E. T. *Liquid-Phase Reaction Rate Constants*; IFI/Plenum: New York, 1974.
(38) *Investigation of Rates and Mechanisms of Reactions*, 4th ed.; Bernasconi C. L., Ed.; John Wiley & Sons: New York, 1986; Vol. VI of *Techniques of Chemistry*.
(39) *Tables of Chemical Kinetics. Homogeneous Reactions*; Thon, N., Ed. National Bureau of Standards, Department of Commerce: Washington DC, 1951.
(40) Beckwith, A. L. J.; Brumby, S.; Claridge, R. F.; Crocket, R.; Roduner, E. In *Radical Reaction Rates in Liquids*; Fischer, H., Ed.; Springer-Verlag: Berlin, 1994; Vol. 18, Subvol. a of *Landolt-Börnstein Numerical Data and Functional Relationships in Sciences and Technology. New Series. Group II, Atomic and Molecular Physics.*
(41) Norton, L. J.; Smigolova, V.; Pralle, M. U.; Hubenko, A.; Dai, K. H.; Kramer, E. J.; Hahn, S.; Berglund, C.; DeKoven, B. *Macromolecules* **1995**, *28*, 1999.
(42) Mader, D.; Coen, M. C.; Kressler, J.; Mulhaupt, R.; Weber, M. *J. Appl. Polym. Sci.* **1997**, *65*, 567−579.
(43) Lambla, M.; Seadan, M. *Polym. Eng. Sci.* **1992**, *32*, 1687.

MA980896G